© 2017. Published by The Company of Biologists Ltd | Journal of Experimental Biology (2017) 220, 4270-4281 doi:10.1242/jeb.164145

RESEARCH ARTICLE

A circuit for detection of interaural time differences in the nucleus laminaris of turtles

Katie L. Willis*,‡ and Catherine E. Carr

ABSTRACT

The physiological hearing range of turtles is approximately 50–1000 Hz, as determined by cochlear microphonics (Wever and Vernon, 1956a). These low frequencies can constrain sound localization, particularly in red-eared slider turtles, which are freshwater turtles with small heads and isolated middle ears. To determine if these turtles were sensitive to interaural time differences (ITDs), we investigated the connections and physiology of their auditory brainstem nuclei. Tract tracing experiments showed that cranial nerve VIII bifurcated to terminate in the first-order nucleus magnocellularis (NM) and nucleus angularis (NA), and the NM projected bilaterally to the nucleus laminaris (NL). As the NL received inputs from each side, we developed an isolated head preparation to examine responses to binaural auditory stimulation. Magnocellularis and laminaris units responded to frequencies from 100 to 600 Hz, and phase-locked reliably to the auditory stimulus. Responses from the NL were binaural, and sensitive to ITD. Measures of characteristic delay revealed best ITDs around ±200 μs, and NL neurons typically had characteristic phases close to 0, consistent with binaural excitation. Thus, turtles encode ITDs within their physiological range, and their auditory brainstem nuclei have similar connections and cell types to other reptiles.

KEY WORDS: Sound localization, Interaural time difference, Turtle, Binaural hearing

INTRODUCTION

Tympana have evolved multiple times in lineages leading to extant amphibians, reptiles and mammals (Clack, 1997, 2002; Willis et al., 2013a; Carr and Christensen-Dalsgaard, 2016). In turtles, adaptations of the tympanum have produced an ear that is somewhat more sensitive underwater than in air, but still adapted to an amphibious lifestyle, as shown both by laser vibrometry measures of tympanum responses in air and water, and by auditory brainstem responses (ABR) in air (Christensen-Dalsgaard et al., 2012; Willis et al., 2013b). In a commonly studied model, the red-eared slider turtle, *Trachemys scripta elegans*, the tympanum is a disc about 0.5 mm thick that moves via a hinged connection to the bony capsule wall surrounding it (Wever and Vernon, 1956b; Christensen-Dalsgaard et al., 2012). In air, sound pressure moves the tympanic disc. When submerged, the air in the middle ear cavity resonates in the underwater sound field, which drives the tympanic disc from within the skull (Christensen-Dalsgaard et al., 2012).

In air, red-eared sliders are relatively insensitive to sound, hearing low frequencies at comparatively high thresholds, mostly below 1 kHz and above 40 dB sound pressure level (SPL) (Christensen-Dalsgaard et al., 2012; review in Manley, 2010). Hair cells in their basilar papilla are tuned to specific frequencies in the acoustic stimulus from near 20 Hz to above 500 Hz, through an electrical resonance mechanism (Crawford and Fettiplace, 1981a,b; Art et al., 1986). Despite the prominence of turtles as a model of hair cell tuning (e.g. Fettiplace and Fuchs, 1999), relatively little is known about their central auditory system (for review, see Willis et al., 2013a), with the notable exception of immunohistochemical studies of the central auditory system in pond turtles (Belekhova et al., 1985, 2002, 2008, 2010). Ethological relevance is added by recent findings that *Chelodina oblonga*, a side-necked, freshwater turtle, emits sounds underwater that may be used for communication (Giles et al., 2009). Finally, the position of testudines relative to other vertebrate taxa has been resolved. Molecular analyses have identified testudines as a sister group to the archosaurs (Shen et al., 2011; Chiari et al., 2012; Lu et al., 2013), a group characterized by sensitive hearing. This newly clarified evolutionary relationship motivated our investigation of the turtle auditory system in order to compare it with that of other reptiles.

In all reptiles, the auditory branch of cranial nerve VIII bifurcates to terminate in the first-order nucleus magnocellularis (NM) and the nucleus angularis (NA). The NM projects bilaterally to the nucleus laminaris (NL). NL and NA then project to the midbrain torus semicircularis (TS) (for reviews, see Carr and Code, 2000; Grothe et al., 2004; Willis et al., 2013a). Previous work on turtles showed that the auditory branch of cranial nerve VIII projected to NM and NA (Marbey and Browner, 1985; Sneary, 1988). Putative NM cell types have also been described in turtles (Browner and Marbey, 1988). However, a difficulty in many of the older studies lay in the identification of nucleus borders. For example, Miller and Kasahara (1979) were not able to identify a clear projection from the NM to the NL, or differentiate between NM and NL. We therefore used more recently developed techniques to define the auditory nuclei and their connections. As turtles have been identified as a sister group to the archosaurs, we hypothesized that connections between their auditory nuclei would follow the archosaurian pattern.

It can be difficult to maintain a stable plane of anaesthesia in turtles without activation of the head withdrawal reflex. In parallel with the tract tracing studies, we therefore developed an isolated head preparation to investigate the physiology of the central auditory system. Crawford and Fettiplace (1981a) had previously developed a half-head preparation for neurophysiological studies of hair cells and the auditory nerve (Crawford and Fettiplace, 1981a, 1983; Art and Fettiplace, 1987; Hailey et al., 1991; Art et al., 1995). The basilar papilla of turtles can be isolated and recorded *in vitro* (e.g. Schnee et al., 2005, 2011, 2013) and models of hair cell

University of Maryland, Department of Biology, Center for Comparative and Evolutionary Biology of Hearing, Neuroscience and Cognitive Science Graduate Program, College Park, MD 20742, USA.
*Present address: University of Oklahoma, Department of Biology, Norman, OK 73019, USA.

‡Author for correspondence (kwillis@ou.edu)

K.L.W., 0000-0002-1046-6184

Received 5 June 2017; Accepted 19 September 2017

Journal of Experimental Biology

Journal of Experimental Biology (2017) 220, 4270-4281 doi:10.1242/jeb.164145

List of abbreviations

ABR	auditory brainstem response
ACSF	artificial cerebrospinal fluid
BF	best frequency
CD	characteristic delay
CP	characteristic phase
IPD	interaural phase difference
ITD	interaural time difference
NA	nucleus angularis
NL	nucleus laminaris
NM	nucleus magnocellularis
SO	superior olive
TS	torus semicircularis

stereocilia have been derived from isolated turtle basilar papilla preparations (Breneman et al., 2009). In other experiments, turtle isolated head or isolated brain regions have been used to examine properties of cerebellum (Rice and Nicholson, 1990) and cortex (Larkum et al., 2008). Turtle cortex is three-layered, and has been studied in a visual cortex preparation that can include the optic nerve and eye (Connors and Kriegstein, 1986; Kriegstein and Connors, 1986; Mancilla et al., 1998; Du et al., 2006). The mitral cells of the turtle olfactory bulb have been studied *in vitro* (Mori et al., 1981). Cortical experiments have used chronically implanted electrodes *in vivo* (Rutishauser et al., 2013) as well as *in vitro* (Rice and Nicholson, 1990; Du et al., 2006).

In the whole head preparation, we used a craniotomy to expose the areas of interest, and dichotic stimulation to test response properties of neurons. In accordance with ABR measurements (Christensen-Dalsgaard et al., 2012), and cochlear potentials (Wever and Vernon, 1956a,c), we hypothesized that the turtle brainstem would be most responsive to frequencies under 1 kHz and encode a small range of ITDs, consistent with its head size.

MATERIALS AND METHODS

All experiments were carried out with the approval and under the guidelines of the University of Maryland Institutional Animal Care and Use Committee, and in accordance with the National Institutes of Health Guide for the Care and Use of Laboratory Animals.

Surgery and anaesthesia

Adult red-eared slider turtles [*Trachemys scripta elegans* (Wied-Neuwied 1839)] of both sexes were obtained from Kons Direct (Germantown, WI, USA). Animals ranged from 10 to 15 cm in carapace length; 10 cm carapace is the minimum size turtle allowed to be sold (Title 21 CFR 1240.62, United States Code of Federal Regulations). Animals were group housed and maintained on a 12 h:12 h light:dark cycle. For anaesthesia before all procedures, propofol (5 mg kg^{-1}; MacLean et al., 2008) was administered intravenously through the subcarapacial vein, which lies immediately below where the neck meets the carapace. After cessation of all reflexes, animals were rapidly decapitated. The brain was exposed to allow for sufficient volume of flow (~1 ml min^{-1}) of oxygenated artificial cerebrospinal fluid (ACSF) composed of 96.5 mmol l^{-1} NaCl, 2.6 mmol l^{-1} KCl, 4.4 mmol l^{-1} $CaCl_2$, 2.0 mmol l^{-1} $MgCl_2$, 31.5 mmol l^{-1} $NaCO_3$ and 10 mmol l^{-1} dextrose dissolved in distilled water (Connors and Kriegstein, 1986).

Tract tracing and Golgi

Neurobiotin (Life Technologies, Grand Island, NY, USA) was applied to brainstem or midbrain structures, using either iontophoresis of 4% neurobiotin in 0.9% saline (1–2 µA alternating positive current for 10 min) or application of neurobiotin on the tip of a tungsten microelectrode (see below). For dye transport, tissue was immersed in a 4°C incubator, with oxygen-saturated ACSF changed every 24 h. Transport time varied from 1 to 96 h; anterograde transport from the NM to the ipsilateral NL was brief (12 h), while retrograde transport from TS to the NA or the NL took longer (2 days). The tissue (midbrain, hindbrain) was immersion-fixed in 4% paraformaldehyde in 0.01 mol l^{-1} phosphate-buffered saline (PBS) for 18–24 h. The brain was then cryoprotected in 30% sucrose in 0.01 mol l^{-1} PBS. Tissue was cut on a freezing microtome in 80 µm sections and rinsed in 0.01 mol l^{-1} PBS. Sections were incubated in avidin biotin complex (ABC kit, Vector Laboratories, Burlingame, CA, USA), in 0.2% Triton in 0.01 mol l^{-1} PBS solution for 1–4 h at room temperature, and then reacted using the Vector SG Peroxidase (HRP) Substrate Kit (Vector Laboratories) for 10–20 min then rinsed with 0.01 mol l^{-1} PBS. Tissue was counterstained with Neutral Red or Cresyl Violet, dehydrated and cleared. Labelled neurons were digitally reconstructed using Neurolucida (MBF Bioscience, Williston, VT, USA). Measurements were made using NeuroExplorer (MBF Bioscience).

The rapid Golgi technique was used on five young turtles (carapace length 2.5 cm) (Valverde, 1970). Brains were removed and placed in Golgi fixative, an aqueous solution containing 2.33% potassium dichromate and 0.19% osmium tetroxide. After one week, the brains were rinsed in 0.75% aqueous silver nitrate, and stored for 24 h in a fresh volume of 0.75% silver nitrate. Brains were then sectioned at 100 µm. Magnocellular and laminaris neurons were found in four brains.

Electrophysiology

The isolated turtle brain preparation offers advantages over traditional *in vivo* and *in vitro* (slice) preparations. Keeping the ear intact enables use of acoustic instead of electrical stimuli, and an isolated head preparation avoids the difficulties of keeping a turtle sufficiently anaesthetized. Maintaining a turtle at the appropriate plane of anaesthesia is difficult because the head withdrawal response may return even with a surgical plane of anaesthesia. This preparation also provides unrestricted access to the dorsal brainstem, normally obscured by a large sinus.

We maintained the preparation at 24–30°C (Table S1), in order to match the temperature at which the animals are housed.

The most effective ACSF was developed by Connors and Kriegstein (1986) (Table S1). These preparations remained responsive for 4–14 h; one preparation was responsive after being immersed in oxygenated ACSF in a 4°C refrigerator overnight. ACSF was bubbled with 95% O_2–5% CO_2 gas for 10 min before initial use and again every 2–3 h. We used an ACSF drip through intravenous (IV) tubing to superfuse the brain. The head was held in a constant position by a stainless-steel head post glued to the prefrontal bone. Recordings were made with 125 µm tungsten microelectrodes (F. Haer, Bowdoin, ME, USA), with impedances around 20 MΩ. Electrodes were positioned above the acoustic tubercle, a prominence of the floor of the lateral recess of the fourth ventricle that contains the primary and secondary auditory nuclei (Fig. 1). Electrodes were advanced remotely in 5–10 µm steps, while continuously testing for auditory responses. Responses were amplified (µA200, Walsh Electronics, Pasadena, CA, USA), high-pass filtered at 300 Hz, and passed through an A/D converter (TDT DD1). Both the analog and the transistor–transistor logic (TTL) signals were stored and processed by custom-written software

Journal of Experimental Biology (2017) 220, 4270-4281 doi:10.1242/jeb.164145

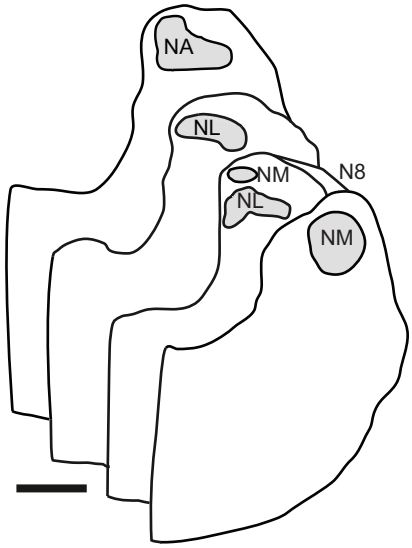

Fig. 1. Rostrocaudal location of the auditory brainstem nuclei. Schematic boundaries of the auditory nuclei in transverse section. The section containing only nucleus angularis (NA) is most rostral; the section containing only the nucleus magnocellularis (NM) is most caudal. N8, cranial nerve VIII. Scale bar,100 μm.

('Xdphys' written in Dr M. Konishi's laboratory at the California Institute of Technology, CA, USA). Recordings were made in a sound-attenuating chamber (IAC Acoustics, North Aurora, IL, USA). Closed, custom-made sound systems were placed around the tympanic disc on both ears, containing commercial miniature earphones and miniature microphones (Knowles EM 3068, Knowles Electronics, Itasca, IL, USA). These were sealed against the head using Gold Velvet II ear impression material (All American Mold Laboratories, Oklahoma City, OK, USA). The sound systems were calibrated individually before the recordings.

Acoustic stimuli were digitally generated by Xdphys, driving a signal-processing system (Tucker Davis Technology, Gainesville, FL, USA). Stimuli were generated separately for the two ears using a TDT AP2 signal-processing board. Both channels were then fed to the earphones via D/A converters (TDT DD1), anti-aliasing filters (TDT FT6-2), and attenuators (TDT PA4). Tone bursts had 100 ms duration (including 5 ms linear ramps) and were presented at a rate of 5 s^{-1} and thus a duty cycle of 50%. We measured monaural iso-level frequency responses and rate-intensity functions at best frequency (BF). Interaural time differences (ITD) were tested within ±1 stimulus period, in steps no larger than 1/10 of the period and stimulus durations of 100 ms. Stimulus levels were between 70 and 85 dB SPL, and 10–15 stimulus repetitions were presented at each ITD.

Only single units were used for ITD analysis (characteristic delay, mean phase). Single units were isolated as distinct spikes above the recording baseline, with the presence of a refractory period in the interspike interval histogram. To calculate characteristic delays (CD), we fitted spike rate as a function of ITD with a cosine function at the respective stimulus frequency to determine best interaural phase difference, or the peak closest to zero interaural phase difference (Viete et al., 1997; MATLAB, MathWorks, Natick, MA, USA). After measuring tonal ITD curves at many frequencies within the frequency response area of a cell, we plotted the mean interaural phase, which represents the peak of the periodic ITD curve in cycles, as a function of frequency. In these plots, the slope of the linear regression is the CD, and the *y*-intercept is the characteristic phase (CP; Yin and Kuwada, 1983). CPs were between 0.25 and −0.25 cycles.

RESULTS

Hindbrain auditory nuclei

On each side, the hindbrain contained four auditory nuclei (Fig. 1) (Miller and Kasahara, 1979; Belekhova et al., 1985). The first-order nuclei, the NA and the NM, were located dorsal and medial in the acoustic tubercle. A second-order nucleus, the NL, was also located in the acoustic tubercle, below the NM. NM, NL, NA, the superior olive (SO) and the torus semicircularis (TS; in the midbrain) were found in similar locations to lizards and birds (reviews in Carr and Code, 2000; Willis et al., 2013a).

All nuclei formed rostrocaudal columns. In Nissl-stained material, the borders of the auditory nuclei could be distinguished in both Cresyl Violet- (Fig. 2A) and Neutral Red-stained material (Figs 2B and 3B,C). From caudal to rostral, the NM was most caudal, and the rostral portion of NM overlapped the caudal portion

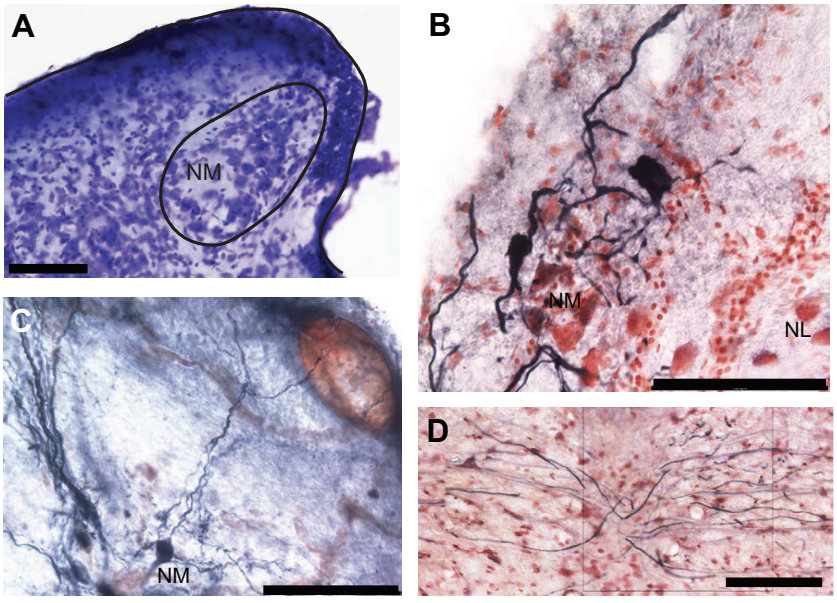

Fig. 2. Nucleus magnocellularis neurons project bilaterally to the nucleus laminaris. (A) Cresyl Violet-stained transverse section of the acoustic tubercle and the nucleus magnocellularis (NM), outlined in black. (B) Retrogradely labelled NM neurons in rostral NM following injection of neurobiotin into the contralateral acoustic tubercle. NL, nucleus laminaris. (C) Retrogradely labelled NM neuron with an ascending dendrite in the cranial nerve VIII tract. (D) Neurobiotin-labelled NM axons in the internal arcuate tract at the midline, just ventral to the fourth ventricle. All scale bars, 100 μm.

Journal of Experimental Biology

Journal of Experimental Biology (2017) 220, 4270-4281 doi:10.1242/jeb.164145

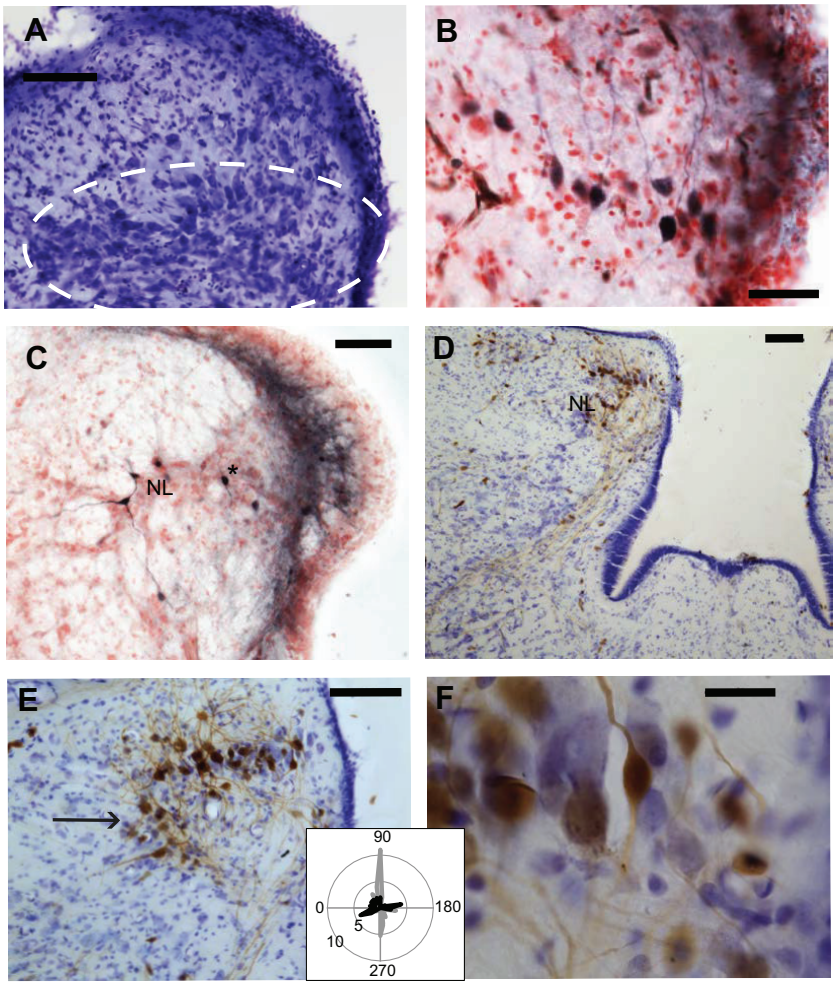

Fig. 3. The nucleus laminaris is primarily composed of vertically oriented, bitufted neurons. (A) Cresyl Violet-stained transverse section through the NL (the dashed white line outlines the NL). (B,C) Retrogradely labelled NL neurons after neurobiotin injection into the torus semicircularis (TS). (D–F) Retrogradely labelled NL neurons after horseradish peroxidase injection into the TS. The arrow in E indicates the ventral bend in lateral NL. (F) Bitufted dendritic morphology in retrogradely labelled NL neurons magnified from D. Scale bar, 20 μm. Inset, polar plot of dendritic orientation reveals bitufted organization (values in deg) in both dorsal and ventral dendrites [*N*=22 neurons from the medial lamina region (grey), *N*=17 from the ventral bend of the lateral region of NL (black)]. Each dendrite has a value of one on the unit circle, with dendritic orientation plotted with respect to the lamina of NL cell bodies. All scale bars, 100 μm (except in F).

of NL. Next, NL was ventral to NM and NA (Fig. 1). The caudal part of NA overlapped the rostral part of NL and lay dorsal to NL. Both the NA and NM were superficial, located on the medial edge of the brainstem below the IV ventricle (Fig. 1). NA was also superficial and medial, caudal to the cerebellar peduncle. In transverse sections, NM was round, while NA had a roughly ovoid shape, but became more round rostrally. Caudally, NA had less defined borders, forming a polygonal outline in reconstructions. NL formed a crescent in transverse section. It was more compact medially and spread out in the dorsoventral axis more laterally. The SO was a round nucleus in the ventral brainstem, below NL (see Fig. 4B).

In addition to position, nuclei were defined by their afferent and efferent connections. Tract tracing experiments revealed the connections of the brainstem nuclei. The NA and the NM received input from the ipsilateral cranial nerve VIII. The details of these projections are the subject of another study (Willis et al., 2014). NM projected bilaterally to NL, and contralaterally projecting NM axons formed a distinctive cross-tract, termed the acoustic stria, above the medial longitudinal fasciculus (Fig. 2D, see Fig. 4 for a summary). After crossing the midline, NM axons ascended into the contralateral acoustic tubercle and arborized in the neuropil below the contralateral NL cell body layer. Neurobiotin injections into NM consistently yielded axons in the acoustic stria and terminals below the NL (*N*=6), while neurobiotin injections into the NL retrogradely labelled neurons in the contralateral NM (53 neurons, *N*=4 cases; Fig. 2B,C). Retrogradely labelled NM neurons were distributed approximately equally among the four cases.

Reconstruction of retrogradely and Golgi-labelled magnocellular neurons revealed cell body areas of about 150 μm^2 (139.9±68.3 μm^2, *N*=70), and a varied number of dendrites (Fig. 2B,C; Fig. 4A). Some magnocellularis neurons appeared to have short or no dendrites, while others had dorsally directed dendritic arbors that penetrated the cranial nerve VIII tract above NM (Fig. 2C). Despite these differences in dendritic arbors, NM appeared to contain a single cell type on the basis of cell body size and form factor. NM cell bodies tended to be rounder (form factor=0.85±0.07) and smaller than NA somata. Using ANOVA, three main features separated the primary and secondary auditory nuclei. NA soma areas were larger than NL or NM (P<0.01, f=18.81, N=189). NA soma form factors were smaller than NM and NL (i.e. NM and NL soma were more round, P<0.05, f=2.32, N=189). Finally, NL average dendrite length was greater than NM and NA (P<0.01, f=21.25, N=189). Both retrogradely labelled neurobiotin-filled neurons and reconstructed Golgi-stained neurons were included in this analysis, which is reflected in the *N* values.

In addition to receiving bilateral projections from the NM, the NL was identified by its rostrocaudal position between the NM and the NA, by the lack of auditory nerve inputs, and by retrograde labelling of its neurons after dye injections confined to the TS. NL neurons formed a lamina that was compact medially and spread laterally (Figs 3 and 4A). This lamina was characterized by bitufted neurons (retrogradely labelled and reconstructed, *N*=45). The NL soma had

Journal of Experimental Biology (2017) 220, 4270-4281 doi:10.1242/jeb.164145

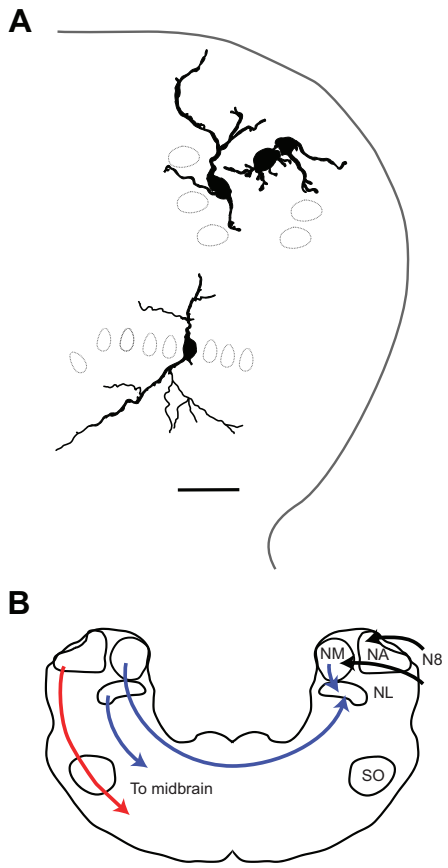

Fig. 4. Summary of auditory circuits. (A) Labelled nucleus magnocellularis (NM; above) and nucleus laminaris (NL; below) neurons from a young turtle, drawn from a single transverse section. Rapid Golgi method (black neurons) with dotted outlines showing positions of unlabelled neurons. The grey line outlines the medial acoustic tubercle. These nuclei are shown in schematic form in B. Scale bar, 100 µm. (B) Circuit diagram summarizing the results of tract tracing experiments. The black arrows mark the auditory nerve input to first-order NM and NA. The blue arrows show the projections of the NM and NL. The superior olive (SO) receives input from NA and NL (not shown). N8, cranial nerve VIII. The red arrow shows the path from the NA to the midbrain. This diagram shows the acoustic tubercle, which is defined as the portion of the brainstem that contains NA, NM and NL.

an average form factor of 0.86±0.1 and an average area of 143.5 ±56.3 µm^2 (N=45). In medial NL, the dendrites of the bitufted neurons were dorsoventrally oriented (Figs 3 and 4A). More laterally, the NL lamina became less compact, neurons tended to spread apart, and their orientation became less strictly dorsoventral (Fig. 3E, arrow). The lateral edge of the NL tended to curve ventrally, and some neurons were separated from the main lamina of the nucleus (Fig. 3C,E). Within the main lamina of NL, the dendrites were bitufted, with dorsal dendrites extending into the NM or dorsal fiber bundles, and ventral dendrites arborizing below laminaris. Measures of dendritic orientation with respect to the lamina of NL cell bodies showed a largely orthogonal orientation (Fig. 3E insert, grey lines), while dendritic orientations in the lateral, curved region of the NL were less strictly oriented (Fig. 3E insert, black lines). NL neurons projected bilaterally to TS, as seen from retrograde labelling using neurobiotin (NB; four cases) and horseradish peroxidase injections into the TS (HRP; two cases) (Figs 3 and 4B).

Dye injection into the TS also labelled ascending lemniscal fibres from the ipsilateral NA and ipsilateral superior olivary nuclei (N=6 cases). The NA and the SO projected to the lemniscal nuclei and to the TS, which forms the dorsal portion of the caudal midbrain, just rostral to the cerebellar peduncles and caudal to the optic tectum. NA projected bilaterally to TS, with the contralateral projection being more prominent than the ipsilateral one. Thus, the brainstem auditory nuclei followed the connectivity pattern previously shown for the pond turtles *Emys orbicularis* and *Testudo horsfieldi* (Belekhova et al., 1985) and for all other reptiles, including birds (Fig. 4B).

Isolated head preparation

In turtles, the ACSF formulation and temperature control were key to obtaining viable recordings (Table S1). The recipe we used was optimized for turtle *in vitro* recordings. The superfusion rates of oxygenated ACSF were similar to the set-up of other *in vitro* physiology experiments. Keeping the preparation warm (25–30°C) by using a commercial space heater to heat the sound-attenuating chamber yielded the largest number of stable recordings. The temperature at which we obtained stable recordings overlapped with the temperature range at which the animals were housed (25–30°C). We began by using the ACSF recipe used in avian slice preparations (e.g. MacLeod and Carr, 2005). Tissue maintained in avian ACSF was healthy enough for dye transport but not for physiological recordings. Another ACSF solution used for one experiment contained 0.005 mol l^{-1} imidazole; the preparation was only viable for about 1 h (two units recorded) with this ACSF (Table S1; Rodgers-Garlick et al., 2013). We also used a solution developed for an *in vitro* turtle cerebellum preparation that contained tetramethylammonium chloride (Rice and Nicholson, 1990), which also yielded viable preparations for about 1 h. We ultimately obtained the best results by regularly oxygenating the solution used by Connors and Kriegstein (1986), and with a perfusion rate of about 1 ml min^{-1} over the surface of the medulla.

Physiological characteristics of nucleus magnocellularis

In the isolated brain preparation, the acoustic tubercle appeared as a well-delineated expansion of the medial wall of the medulla. Recordings from the isolated brain preparation provided data on responses to auditory stimulation in NM. We report the frequency tuning, phase-locking and responses to increasing sound intensity of 123 NM units from 29 animals, recorded from the dorsal portion of the acoustic tubercle, with depths from the brain surface in the range 107±82 µmm (N=101). NM units only responded to ipsilateral sound and could therefore be differentiated from NL responses. SPL used were typically within 10 to 20 dB above threshold at each frequency. Best frequencies in NM ranged from 100 to 600 Hz (Fig. 5). Auditory thresholds measured at BF revealed mean thresholds of 69.2±9.12 dB SPL (N=123, Fig. 5B,C). The lowest recorded single-unit thresholds were 40 dB SPL for three units, with best frequencies of 150, 220 and 400 Hz, respectively. Average physiological thresholds were high compared with other reptiles, and also above thresholds recorded *in vivo* from the common box turtle (mean of 48±8 dB SPL, N=24, measured from fig. 1 of Manley, 1970). Thresholds were generally similar to, but below, the thresholds derived from ABR audiograms (Fig. 5; Christensen-Dalsgaard et al., 2012).

NM units reliably phase-locked to the stimulus (Fig. 6, sample phase histogram in 6A, inset). Phase-locking is measured using a period histogram (Fig. 6A, inset), which plots the instantaneous firing rate as a function of stimulus phase in cycles. The degree of phase-locking is typically quantified using the metric of vector strength (Goldberg and Brown, 1969; Ashida and Carr, 2010).

Journal of Experimental Biology

Journal of Experimental Biology (2017) 220, 4270-4281 doi:10.1242/jeb.164145

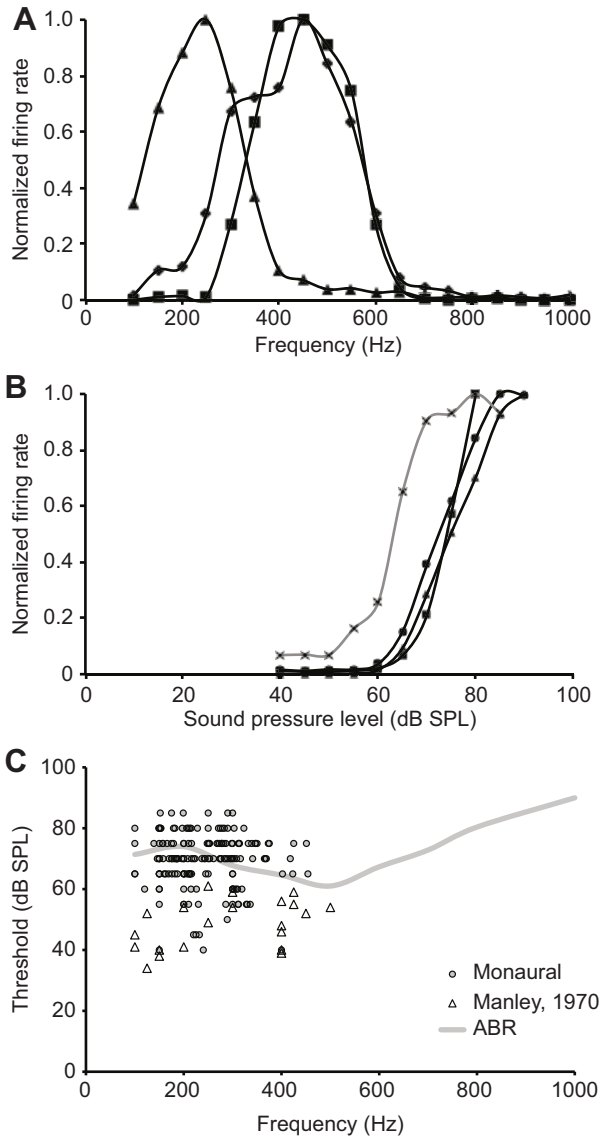

Fig. 5. Physiological properties of NM neurons. (A) Representative constant intensity (80 dB) frequency–rate curves for three NM neurons with best frequencies (BFs) between 200 and 500 Hz. (B) Rate intensity functions of the neurons shown in A, measured at BF, as well as a lower threshold example (grey ×, BF=355 Hz). BFs for symbols in A and B: triangle, 226 Hz; diamond, 424 Hz; square, 475 Hz). (C) Threshold measured at BF in NM single units with ABR audiogram (Christensen-Dalsgaard et al., 2012) and *in vivo* cochlear nucleus data for comparison (Manley, 1970).

Vector strength falls between 1 (all spikes in a single bin) and 0 (no phase-locking). In the turtle recordings, phase-locking was measured at BF. We observed almost no changes in vector strength with frequency (Fig. 6A). In NM, phase-locking vector strength varied from 0.53 to 0.97, averaging 0.82±0.07 (N=123). Firing patterns tended to be primary-like (Fig. 6B), characterized by a phasic peak of activity at the beginning of the stimulation, followed by a tonic discharge at a lower rate for the rest of the stimulus period. We also recorded units with more sustained responses to stimulation (Fig. 6C,D).

Fig. 6C,D shows responses from a magnocellularis neuron, with a BF of 180 Hz, to a 100 ms tone. The dot raster (Fig. 6C) indicates the occurrence of spikes, relative to the stimulus, upon 50 repeated presentations of the same tone (see Joris et al., 2006). The vertical patterning of the dots show that spikes occur at a preferred phase of the stimulus. This is more easily seen in the post-stimulus time histogram (Fig. 6D) in which the spikes from this neuron are aligned with the onset, or a fixed phase point, of an identical stimulus presented 100 times. The aligned sequences are superimposed in time, and then used to construct a histogram. Measurements of the interspike intervals (Fig. 6D, inset) show the expected stimulus period of 5.55 ms associated with stimulation at 180 Hz.

Physiological characteristics of nucleus laminaris

We recorded from NL units in the dorsal portion of the acoustic tubercle in 13 different animals, both below NM and sometimes more rostral than NM (mean depths of 210±73 µm, N=45). Physiologically, NL units were defined by responses to stimulation of both the ipsilateral and contralateral ears, and were sensitive to interaural time differences (ITD). While we obtained both single (N=45) and multi-unit (N=20) recordings in NL, we did not include multi-units in our measurements of ITD. In order to determine the frequency-independent ITD, we measured ITDs in a range of different frequencies within the frequency response area of a cell, and plotted the mean interaural phase, which represents the peak of the periodic ITD curve in cycles, as a function of frequency. In these plots, the slope of the linear regression is the CD, while the y-intercept is the characteristic phase (CP). Not all 45 NL recordings included all measurements. We have 21 complete data sets with ipsi-, contra- and binaural measurements of BF, threshold, vector strength, ITD sensitivity and CD.

We report the frequency tuning, phase-locking, and responses to increasing sound intensity of NL units. Auditory thresholds measured at BF were generally similar to thresholds in NM, and typically below the thresholds derived from ABR audiograms (Fig. 7A). Units had a mean threshold of 71.2±8.27 dB SPL (N=40; Fig. 7A). The lowest single unit threshold was 55 dB SPL. In NL, recorded best frequencies ranged from 100 to 700 Hz (Fig. 7). In general, NL units responded similarly to stimulation of either ear. In six cases, however, the NL units had lower thresholds and stronger responses to ipsilateral broadband noise than to a particular frequency. All contralateral inputs to NL units were tuned to a particular frequency, and in these cases, the contralateral BF was used to drive the neuron for measures of phase-locking, sensitivity to changes in level, and responses to changing ITD.

Neurons in the NL were sensitive to ITD over a range of frequencies around their BF (Fig. 8). NL units reliably phase-locked to both ipsilateral and contralateral stimuli (Fig. 8D). We measured phase-locking at BF, and at 20 dB SPL above threshold, and found almost no changes in vector strength with frequency (Fig. 7B). In NL, phase-locking vector strength from single units varied from 0.22 to 0.97, averaging 0.79±0.06 (N=45) (Fig. 7B; sample phase histograms in Fig. 8D). NL firing patterns tended to be sustained (Figs 7C,D and 8B). We used monaural phase-locked responses to compute peak phase differences between ipsi- and contralateral period histograms. These phase differences reflected each NL neuron's best ITD (Fig. 8F). NL neurons were excited by both ears; i.e. they were 'peak-type' neurons, with measures of characteristic phase (CP) typically close to 1 or 0, with the CP defined as the phase intercept at 0 Hz in plots of mean interaural phase versus stimulus frequency of the response (Yin and Kuwada, 1983; Kuwada et al., 1987; Fig. 8E, inset). Peak-type neurons displayed ITD functions where the peaks (maxima) were aligned at a particular ITD across frequency (CPs between 0.0 and ±0.25 cycles). CPs averaged −0.025±0.038 (N=21) (Fig. 8D, inset). We calculated fewer CDs than best ITDs because we

Journal of Experimental Biology (2017) 220, 4270-4281 doi:10.1242/jeb.164145

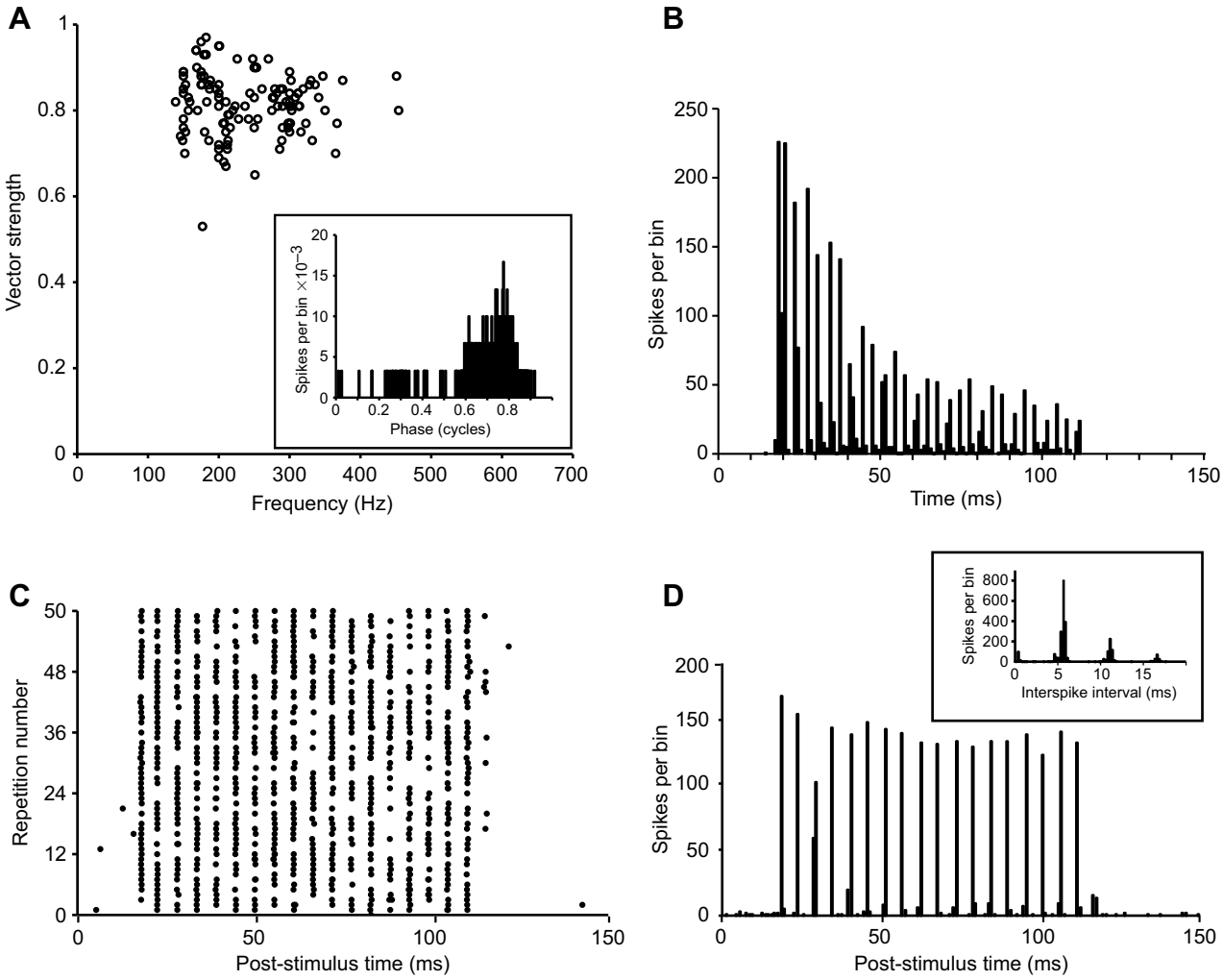

Fig. 6. Phase-locking properties of NM neurons. (A) Vector strengths (VS) of single-unit NM neurons; inset: example phase histogram of a NM neuron, BF=150 Hz, VS=0.88. (B) NM post-stimulus time histogram (PSTH) with primary-like discharge pattern, BF=251 Hz. (C) Dot raster plot from 65 repetitions of stimulus to a NM neuron, BF=180 Hz, VS=0.97. (D) PSTH from the same NM neuron in as in C; inset: interval histogram from same unit.

did not have a sufficient range of frequencies (minimum of five different frequencies for CD calculation) for CD for all recordings.

We performed a detailed analysis of the sensitivity to ITDs in the fine structure of low-frequency pure tones in the subset of 21 NL neurons for which we were able to obtain a complete set of recordings (Fig. 9). Our measures of CD showed that turtles were sensitive to ITDs from −200 to 200 µs, with best ITDs centred on 0 µs (mean −9±68 µs, N=21, where positive ITDs represent the ipsilateral ear) (Fig. 9). These peaks were generally within or close to the physical range of ITDs available to red-eared sliders, which have fairly small heads and ears that are not coupled (Willis et al., 2013b). For estimates of the physical range available to red-eared slider turtles, we used the range of ITDs possible for a large animal (12 inch or 30.5 cm carapace, about 6 cm head width), and the speed of sound in air. We note, however, that we recorded from medium-sized turtles, with a maximum head width of 32 mm. The distribution of recorded ITDs showed a slight asymmetry towards negative values, i.e. to sound originating from the contralateral hemisphere (Fig. 9B,C).

DISCUSSION

We developed an isolated head preparation to analyse neural circuits in the auditory brainstem of the red-eared slider turtle. Recordings from the first-order NM and its target, the NL, revealed neurons sensitive to best frequencies between 100 and 600 Hz, which phase-locked to the auditory stimulus. Best ITDs recorded in the NL were consistent with the turtle's physiological range, or range of time differences determined from their interaural distance.

ITDs conformed to the range of time differences predicted by head size

This is the first demonstration of neural sensitivity to ITDs in turtles, and suggests that they may be able to localize sound sources, albeit poorly. Our data suggest that the largely homogeneous and broadly tuned ITD-sensitive population of neurons in turtle laminaris could encode spatial position by changes in spike rate across the span of physiological ITDs. Turtle neurons have low best frequencies, with the lowest BF neurons having, necessarily, the broadest ITD functions in response to interaurally delayed signals. Thus, even for relatively large changes in ITD, encompassing perhaps the entire range experienced by an animal like the red-eared slider turtle, the response near the peak of the function may change only slightly (Fig. 9A).

Two strategies have emerged to improve localization when low-frequency hearing and small heads limit animals' ability to encode sound source location. Other reptiles, such as lizards and

Journal of Experimental Biology (2017) 220, 4270-4281 doi:10.1242/jeb.164145

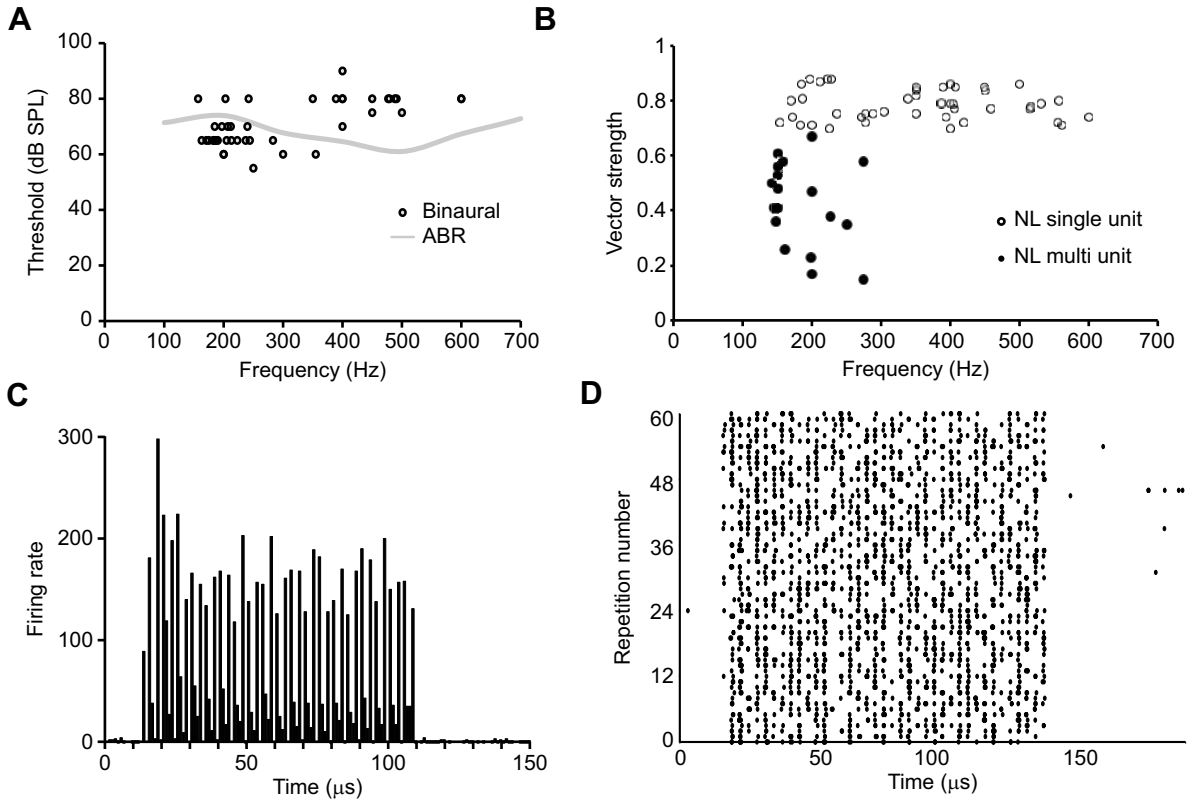

Fig. 7. Physiological properties of NL neurons. (A) Response thresholds measured at BF for all monaural (NM; open circles, *N*=161) and binaural (NL; filled circles, *N*=18) single units recorded. (B) Vector strengths measured at BF in single units (open circles) and multi-units (filled circles). (C) PSTH of a single NL unit at its BF (400 Hz). (D) Dot raster plot from 65 repetitions of the stimulus in C.

archosaurs, have coupled ears, which increase the range of ITDs available at low frequencies (Calford and Piddington, 1988; Christensen-Dalsgaard and Manley, 2008; Carr and Christensen-Dalsgaard, 2016; Carr et al., 2016; Larsen et al., 2016; van Hemmen et al., 2016). Small mammals, such as the gerbil and guinea-pig, show a trend that places the sensitive slope of the function where greatest ITD discrimination is required (McAlpine et al., 2001; for reviews see Grothe et al., 2010; Grothe and Pecka, 2014). By shifting the peak ITD closer to zero for neurons as characteristic frequency increases, the position of the slope through the range of relevant ITDs is maintained. Neither strategy applies to the data presented here, as turtle ears are not coupled and our recordings show ITD peaks largely within their physiological range in air (Fig. 9C).

The combination of small head size, low-frequency hearing and uncoupled ears should make it difficult for the turtle NL to encode a range of ITDs in air. The wavelength of sounds below 1 kHz is much greater than the turtle head size, with wavelengths of 100 Hz in water being about 3.4 m, and about 70 cm in air. Turtle ears are not acoustically coupled, and their middle ears are connected to the pharynx by thin Eustachian tubes (Willis et al., 2013b). Middle ears that are not coupled may be an adaptation for hearing underwater (Christensen-Dalsgaard et al., 2012; Willis et al., 2013a,b). Turtle ITD sensitivity may, however, allow these animals to navigate towards or away from sound sources.

In addition to sound source localization, at least some turtles emit sounds, possibly for communication. *Chelonidina oblonga* emits sound under water, with both percussive and complex calls (Giles et al., 2009). There are also studies suggesting that hatchlings of multiple species vocalize (Ferrara et al., 2013, 2014a,b, 2017). Multiple species of tortoise vocalize during mating (e.g. Campbell and Evans, 1967). Although there are no audiograms (behavioural or derived from physiological tests, like ABR) for most of these species, published audiograms for testudines show a hearing range below 1 kHz with lowest thresholds around 300–600 Hz.

Although the increased speed of sound in water should further reduce the turtle's range of ITDs, most best ITDs in air were close to 0 μs, so if both ears are driven together underwater, best ITDs should remain clustered near 0 μs. It is unlikely that turtles could use the underwater localization cues available to bony fishes, where sound source localization depends upon arrays of hair cells with different orientations (for review, see Edds-Walton, 2016). Scanning electron microscopic studies showed that the hair cells of turtle papillae are unidirectional (Miller, 1978). Miller describes the papillae of turtles as relatively large and characterized by a long, horizontal middle section resting on a wide basilar membrane (Miller, 1978).

Organization of turtle brainstem circuits consistent with phylogeny

Understanding of the low-frequency hearing of testudines may be complicated by their adaptation to hearing underwater (Christensen-Dalsgaard et al., 2012; Willis et al., 2013b). As sound travels much faster in water than in air, hearing underwater might have effects on neural processing that may not be revealed by anatomical experiments, or by physiological studies in air. Nevertheless, the neural circuits described here share similar connections and cell types to other reptiles, including birds. The auditory nerve bifurcates to terminate in the NM and the NA, while the NM projects bilaterally to the NL. NL and NA then project to the midbrain TS

Journal of Experimental Biology (2017) 220, 4270-4281 doi:10.1242/jeb.164145

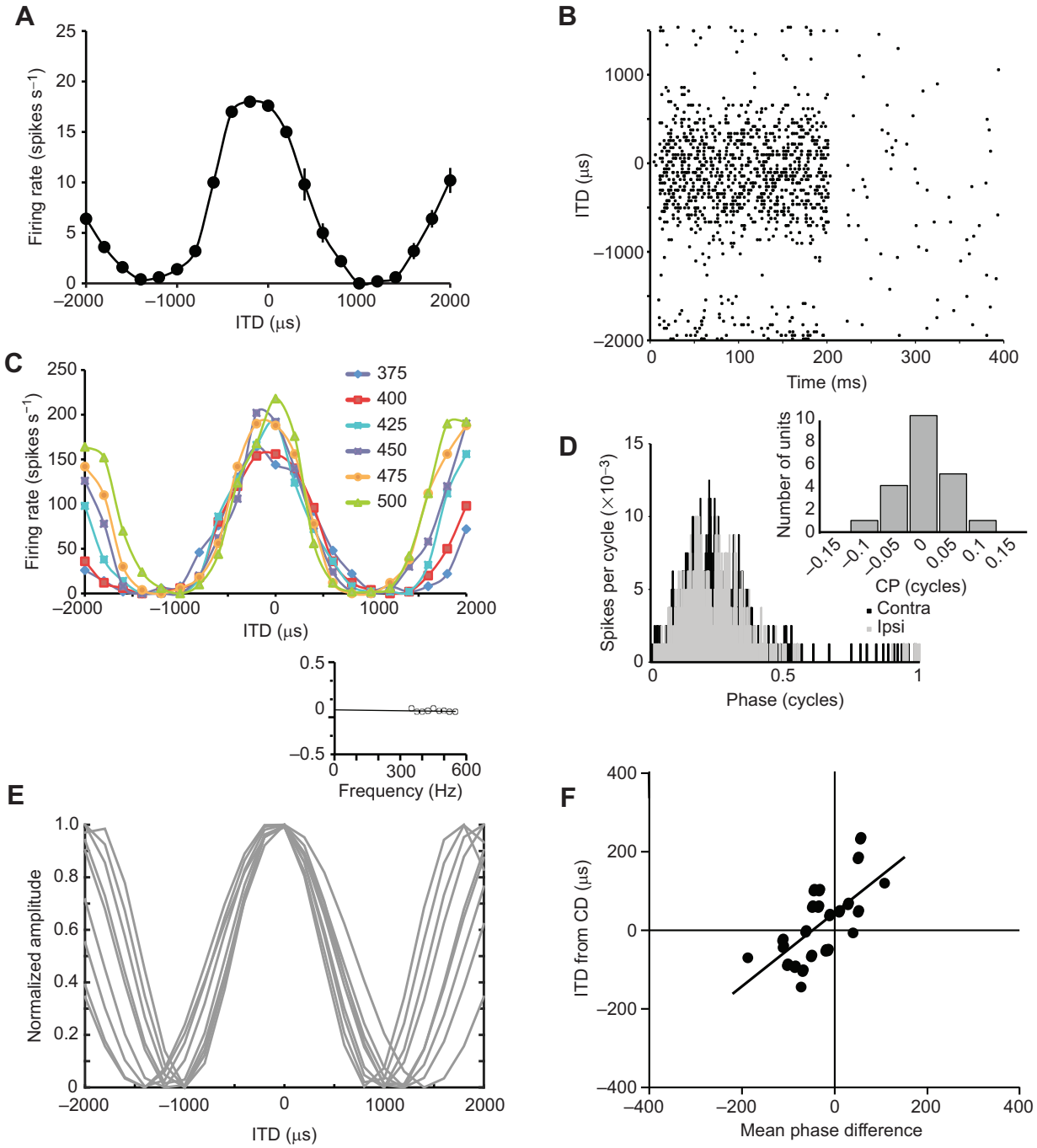

Fig. 8. Turtle NL neurons are sensitive to interaural time difference. (A) Response of a NL single unit to varying ITD at 400 Hz. (B) Raster plot from the same unit. (C) ITD responses recorded in NL as a function of stimulus frequency (BF=425 Hz). Interaural delay curves plot the response of this unit for a range of frequencies from 375 to 500 Hz. Equation for characteristic delay (CD) is $y=-0.000136x+0.017$; $r^2=0.97$. (D) Period histograms of an ITD-sensitive neuron in response to monaural contralateral (black) and ipsilateral (grey) stimulation at 400 Hz. The difference between ipsilateral (left, black, mean phase 0.220, VS=0.81) and contralateral (right, grey, mean phase 0.218, VS=0.77) phase was −5 µs, while binaural stimulation yielded a best ITD of −44 µs. Inset: distribution of characteristic phase (CP) for all NL single units yields a mean CP of −0.01±0.08 (N=43), showing that the inputs to the cell at the CD are in phase. (E) Computation of CD for a single unit in left-hand side NL, BF=450 Hz. Each curve was normalized and fitted with a cosine for the nine frequencies tested, to yield a CD of −84 µs. Inset: best IPD (in cycles) determined for each of the curves shown in E, as a function of stimulation frequency (Hz); the continuous line shows the linear regression. The slope of the line represents the CD, and the y-intercept the characteristic phase (CP); $y=-0.000084x+0.012$; $r^2=0.15$. (F) If laminaris neurons are excited by input from each side, and act as coincidence detectors, then differences between left and right mean phase should predict best ITD. A regression line was drawn for all data ($y=1.0132x+56.89$; $r^2=0.62$).

(for reviews, see Carr and Code, 2000; Grothe et al., 2004; Willis et al., 2013a).

In birds, lizards and mammals, which have a wider range of hearing frequencies than turtles, the brainstem nuclei appear proportionally larger in size. For example, in birds and lizards, the NA is more differentiated than in turtles, with several neuron types (for reviews, see Szpir et al., 1995; Soares and Carr, 2001; Grothe et al., 2004). In our material, measurements of neuron size, number and orientation of

Journal of Experimental Biology (2017) 220, 4270-4281 doi:10.1242/jeb.164145

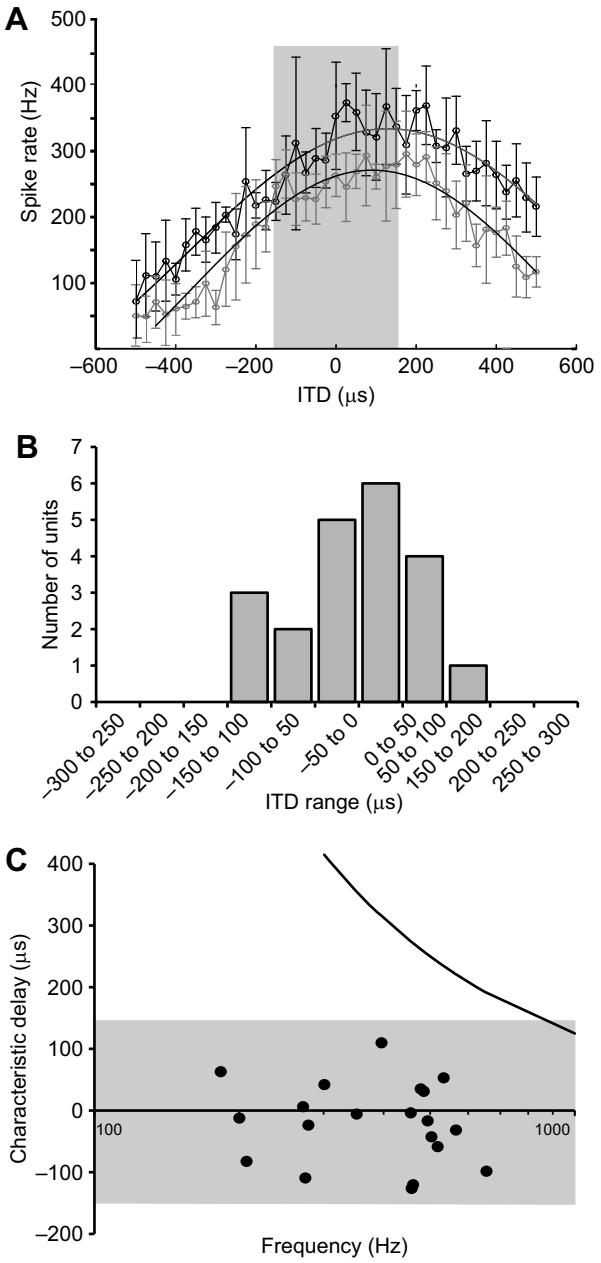

Fig. 9. The majority of ITDs fall within the predicted physiological range. (A) Section of a response of an NL single unit to varying ITD at 500 Hz (grey curve) and 550 Hz (black curve), measured at 25 μs intervals, with five repetitions (±s.e.m.). The grey rectangle (±150 μs) designates the likely physical range available to a large red-eared slider. (B) Distribution of all best ITDs, shown as if measured from the right-hand side NL, 50 μs bins. (C) Distribution of calculated CDs from all NL single units, as if measured from the right-hand side NL. The grey area (±150 μs) designates the likely physical range available to a turtle, and the black line shows the function (best ITD=0.125/BF) (Grothe et al., 2010).

dendrites, and form factor of reconstructed neurons did not reveal different cell types within either the NM or NA. One option for differentiating neurons further would be to use immunohistochemical techniques, expanding on the work of Belekhova et al. (2002), who examined calcium-binding protein expression in turtle auditory structures. Belekhova and coworkers found parvalbumin, calbindin and calretinin immunoreactivity in NM, NA and NL (Belekhova et al., 2008) and in TS (Belekhova et al., 2010).

Multiple theories have been put forward to explain the emergence of diverse neuronal structure–function relationships. One explanation is that specific cell types differentiate to process specific parallel streams of information. Increases in high-frequency sensitivity in lepidosaurs (Manley, 2002) and in other archosaurs, such as birds and crocodilians, may have increased selection for neurons to differentiate in the NA in order to process parallel streams of information. In order to support or refute this hypothesis, recordings from turtle NA are necessary. If the addition of higher frequency hearing drives differentiation into multiple cell types, turtles might more closely resemble the archosaur ancestral condition, as there is no evidence that the common ancestors of archosaurs were auditory specialists. It is more likely that early archosaurs were sensitive to low-frequency sound (Gleich et al., 2004), as is the case for turtles.

Best frequencies and thresholds in the isolated head preparation

Isolated neural preparations have been developed in a variety of animals, including many invertebrates. Some of these leave relevant peripheral structures intact. In mammals, isolated brain preparations are generally maintained by perfusion through the basilar artery with a blood substitute or ACSF (Llinás and Mühlethaler, 1988). In other cases, the isolated tissue is typically submerged in ACSF or saline. The time over which this preparation remains viable depends largely on the species.

The range of best frequencies recorded in the isolated turtle brain preparation was consistent with published ABR audiograms (Christensen-Dalsgaard et al., 2012), suggesting that the isolated preparation was viable. We recorded responses from 100 to 800 Hz; the highest single-unit BF recorded in NM was 454 Hz, and the highest BF multiunit response was 620 Hz. In NL, the highest BF single unit recorded was 600 Hz. These values were similar to recordings from the auditory brainstem of an intact anaesthetized *Terrapene carolina* (common box turtle; Manley, 1970), where 500 Hz was the highest characteristic frequency (Fig. 5C). Thus, *in vivo* recordings yielded similar BF responses to those from our isolated brain preparations.

Similar BF ranges of 100–400 Hz were recorded in prior isolated brain experiments in turtles (Hailey et al., 1991). Although it was possible that higher temperatures might yield higher best frequencies, Hailey et al. (1991) used temperatures up to 40°C and found no units with a BF above 400 Hz. Similar results were obtained from an isolated half-head preparation, where Crawford and Fettiplace (1980) recorded auditory nerve units with best frequencies of 50–700 Hz, and minimum thresholds of 35 dB SPL. In the half-head preparation, both hair cells and auditory nerve fibres yielded sharp tuning curves up to 600 Hz (Crawford and Fettiplace, 1980; Wu and Fettiplace, 1996). To both acoustical and mechanical displacement of hair cells, the auditory nerve responded best below 500 Hz, but could respond to high-intensity stimulation (90–100 dB SPL) up to 1 kHz (Crawford and Fettiplace, 1983).

The *in vivo* recordings made by Manley (1970) yielded similar but more sensitive responses to those from our isolated brain preparation. The lowest thresholds recorded from the cochlear nucleus of an intact anaesthetized *T. carolina* (Manley, 1970) were about 35 dB [mean *in vivo* thresholds computed from Manley (1970); Fig. 1, 48±8 dB, N=23; Fig. 5C]. These values were comparable to the best sensitivities in *Trachemys* auditory nerve of just under 40 dB SPL (Art and Fettiplace, 1986), and comparable only to our best sensitivities of 40 dB SPL, suggesting that the *in vivo* preparation was more sensitive than the isolated brain preparation. Mean sensitivities from *Trachemys* NM were almost

20 dB higher than values recorded *in vivo* from *Terrapene* (69.2±9.12 vs 48±8 dB SPL). The lowest recorded single-unit thresholds from the isolated brain preparation were 40 dB SPL, for three units, with best frequencies of 150, 220 and 400 Hz, respectively.

In all turtle studies, the lowest thresholds occurred at frequencies from 150 to 500 Hz. Compared with other reptiles (and birds), turtles had high thresholds and low best frequencies.

Acknowledgements
We gratefully acknowledge Catherine McCormick for expert advice and for generously providing her anatomical material, Angeline Johny for assistance with histology, and Christina O'Brien for histology and physiology assistance. We also thank Ellengene Peterson for the loan of her anatomical material, and Jose Peña for the MATLAB scripts used for analysis of characteristic delay. We are grateful for the comments of the reviewers, which have greatly improved this paper.

Competing interests
The authors declare no competing or financial interests.

Author contributions
Conceptualization: K.L.W., C.E.C.; Methodology: K.L.W., C.E.C.; Formal analysis: K.L.W., C.E.C.; Writing - original draft: K.L.W., C.E.C.; Writing - review & editing: K.L.W., C.E.C.; Visualization: K.L.W., C.E.C.; Supervision: C.E.C.; Project administration: C.E.C.; Funding acquisition: C.E.C.

Funding
Supported by the National Institute of Deafness and Other Communication Disorders [NIH DC00436 to C.E.C., and NIH DC0466 to the University of Maryland Center for the Evolutionary Biology of Hearing]. Deposited in PMC for release after 12 months.

Supplementary information
Supplementary information available online at
http://jeb.biologists.org/lookup/doi/10.1242/jeb.164145.supplemental

References

Art, J. J. and Fettiplace, R. (1987). Variation of membrane properties in hair cells isolated from the turtle cochlea. *J. Physiol.* **385**, 207-242.
Art, J. J., Crawford, A. C. and Fettiplace, R. (1986). Electrical resonance and membrane currents in turtle cochlear hair cells. *Hear. Res.* **22**, 31-36.
Art, J. J., Wu, Y.-C. and Fettiplace, R. (1995). The calcium-activated potassium channels of turtle hair cells. *J. Gen. Physiol.* **105**, 49-72.
Ashida, G. and Carr, C. E. (2010). Effect of sampling frequency on the measurement of phase-locked action potentials. *Front. Neurosci.* **4**, 172.
Belekhova, M. G., Zharskaja, V. D., Khachunts, A. S., Gaidanenko, G. V. and Tumanova, N. L. (1985). Connections of the mesencephalic, thalamic and telencephalic auditory centers in turtles: some structural bases for audiosomatic interrelations. *J. Hirnforschung* **26**, 127-152.
Belekhova, M. G., Kenigfest-Rio, N. B., Vesselkin, N. P., Rio, J.-P., Repérant, J. and Ward, R. (2002). Evolutionary significance of different neurochemical organisation of the internal and external regions of auditory centres in the reptilian brain: an immunocytochemical and reduced NADPH-diaphorase histochemical study in turtles. *Brain Res.* **925**, 100-106.
Belekhova, M. G., Chudinova, T. V., Kenigfest, N. B. and Krasnoshchekova, E. I. (2008). Distribution of metabolic activity (cytochrome oxidase) and immunoreactivity to calcium-binding proteins in the turtle brainstem auditory nuclei. *J. Evol. Biochem. Phys.* **44**, 354-364.
Belekhova, M. G., Chudinova, T. V., Repérant, J., Ward, R., Jay, B., Vesselkin, N. P. and Kenigfest, N. B. (2010). Core-and-belt organisation of the mesencephalic and forebrain auditory centres in turtles: expression of calcium-binding proteins and metabolic activity. *Brain Res.* **1345**, 84-102.
Breneman, K. D., Highstein, S. M., Boyle, R. D. and Rabbitt, R. D. (2009). The passive cable properties of hair cell stereocilia and their contribution to somatic capacitance measurements. *Biophys. J.* **96**, 1-8.
Browner, R. H. and Marbey, D. (1988). The nucleus magnocellularis in the red-eared turtle, *Chrysemys scripta elegans*: eighth nerve endings and neuronal types. *Hear. Res.* **33**, 257-271.
Calford, M. B. and Piddington, R. W. (1988). Avian interaural canal enhances interaural delay. *J. Comp. Physiol. A* **162**, 503-510.
Campbell, H. W. and Evans, W. E. (1967). Sound production in two species of tortoises. *Herpetologica* **23**, 204-209.
Carr, C. E. and Christensen-Dalsgaard, J. (2016). Evolutionary trends in directional hearing. *Curr. Opin. Neurobiol.* **40**, 111-117.
Carr, C. E. and Code, R. A. (2000). Central auditory system of birds and reptiles. In *Comparative Hearing: Birds and Reptiles* (ed. A. N. Popper, R. R. Fay and R. J. Dooling), pp. 197-248. New York: Springer.
Carr, C. E., Christensen-Dalsgaard, J. and Bierman, H. (2016). Coupled ears in lizards and crocodilians. *Biol. Cybern.* **110**, 291-302.
Chiari, Y., Cahais, V., Galtier, N. and Delsuc, F. (2012). Phylogenomic analyses support the position of turtles as the sister group of birds and crocodiles (Archosauria). *BMC Biol.* **10**, 65.
Christensen-Dalsgaard, J. and Manley, G. A. (2008). Acoustical coupling of lizard eardrums. *J. Assoc. Res. Otolaryngol.* **9**, 407-416.
Christensen-Dalsgaard, J., Brandt, C., Willis, K. L., Christensen, C. B., Ketten, D., Edds-Walton, P., Fay, R. R., Madsen, P. T. and Carr, C. E. (2012). Specialization for underwater hearing by the tympanic middle ear of the turtle, *Trachemys scripta elegans*. *Proc. R. Soc. B* **279**, 2816-2824.
Clack, J. A. (1997). The evolution of tetrapod ears and the fossil record. *Brain Behav. Evol.* **50**, 198-212.
Clack, J. A. (2002). Patterns and processes in the early evolution of the tetrapod ear. *J. Neurobiol.* **53**, 251-264.
Connors, B. W. and Kriegstein, A. R. (1986). Cellular physiology of the turtle visual cortex: distinctive properties of pyramidal and stellate neurons. *J. Neurosci.* **6**, 164-177.
Crawford, A. C. and Fettiplace, R. (1980). The frequency selectivity of auditory nerve fibres and hair cells in the cochlea of the turtle. *J. Physiol.* **306**, 79-125.
Crawford, A. C. and Fettiplace, R. (1981a). Non-linearities in the responses of turtle hair cells. *J. Physiol.* **315**, 317-338.
Crawford, A. C. and Fettiplace, R. (1981b). An electrical tuning mechanism in turtle cochlear hair cells. *J. Physiol.* **312**, 377-412.
Crawford, A. C. and Fettiplace, R. (1983). Auditory nerve responses to imposed displacements of the turtle basilar membrane. *Hear. Res.* **12**, 199-208.
Du, X., Ghosh, B. K. and Ulinski, P. (2006). Encoding of motion targets by waves in turtle visual cortex. *IEEE Trans. Biomed. Eng.* **53**, 1688-1695.
Edds-Walton, P. L. (2016). What the toadfish ear tells the toadfish brain about sound. In *Fish Hearing and Bioacoustics* (ed. J. Sisneros), pp. 197-226. Zurich: Springer.
Ferrara, C. R., Vogt, R. C. and Sousa-Lima, R. S. (2013). Turtle vocalizations as the first evidence of posthatching parental care in chelonians. *J. Comp. Psychol.* **127**, 24-32.
Ferrara, C. R., Mortimer, J. A. and Vogt, R. C. (2014a). First evidence that hatchlings of *Chelonia mydas* emit sounds. *Copeia* **2014**, 245-247.
Ferrara, C. R., Vogt, R. C., Harfush, M. R., Sousa-Lima, R. S., Albavera, E. and Tavera, A. (2014b). First evidence of leatherback turtle (*Dermochelys coriacea*) embryos and hatchlings emitting sounds. *Chelonian Conserv. Biol.* **13**, 110-114.
Ferrara, C. R., Vogt, R. C., Eisemberg, C. C. and Doody, J. S. (2017). First evidence of the pig-nosed turtle (*Carettochelys insculpta*) vocalizing underwater. *Copeia* **105**, 29-32.
Fettiplace, R. and Fuchs, P. A. (1999). Mechanisms of hair cell tuning. *Annu. Rev. Physiol.* **61**, 809-834.
Giles, J. C., Davis, J. A., McCauley, R. D. and Kuchling, G. (2009). Voice of the turtle: the underwater acoustic repertoire of the long-necked freshwater turtle, *Chelodina oblonga*. *J. Acoust. Soc. Am.* **126**, 434-443.
Gleich, O., Fischer, F. P., Koppl, C. and Manley, G. A. (2004). Hearing organ evolution and specialization: Archosaurs. In *Evolution of the Vertebrate Auditory System* (ed. G. A. Manley, A. N. Popper and R. R. Fay), pp. 224-255. New York: Springer.
Goldberg, J. M. and Brown, P. B. (1969). Response of binaural neurons of dog superior olivary complex to dichotic tonal stimuli: some physiological mechanisms of sound localization. *J. Neurophysiol.* **32**, 613-636.
Grothe, B. and Pecka, M. (2014). The natural history of sound localization in mammals – a story of neuronal inhibition. *Front. Neural Circuits* **8**, 116.
Grothe, B., Carr, C. E., Casseday, J. H., Fritzsch, B. and Koppl, C. (2004). The evolution of central pathways and their neural processing patterns. In *Evolution of the Vertebrate Auditory System* (ed. G. A. Manley, A. N. Popper and R. R. Fay), pp. 289-359. New York: Springer.
Grothe, B., Pecka, M. and McAlpine, D. (2010). Mechanisms of sound localization in mammals. *Physiol. Rev.* **90**, 983-1012.
Hailey, A., Rosenberg, M. E. and Pullen, A. H. (1991). An *in vitro* brainstem preparation preserving peripheral auditory function. *J. Neurosci. Meth.* **39**, 217-223.
Joris, P. X., Louage, D. H., Cardoen, L. and van der Heijden, M. (2006). Correlation index: a new metric to quantify temporal coding. *Hear. Res.* **216-217**, 19-30.
Kriegstein, A. R. and Connors, B. W. (1986). Cellular physiology of the turtle visual cortex: synaptic properties and intrinsic circuitry. *J. Neurosci.* **6**, 178-191.
Kuwada, S., Stanford, T. R. and Batra, R. (1987). Interaural phase-sensitive units in the inferior colliculus of the unanesthetized rabbit: effects of changing frequency. *J. Neurophysiol.* **57**, 1338-1360.
Larkum, M. E., Watanabe, S., Lasser-Ross, N., Rhodes, P. and Ross, W. N. (2008). Dendritic properties of turtle pyramidal neurons. *J. Neurophysiol.* **99**, 683-694.

Larsen, O. N., Christensen-Dalsgaard, J. and Jensen, K. K. (2016). Role of intracranial cavities in avian directional hearing. *Biol. Cybern.* **110**, 319-331.
Llinás, R. and Mühlethaler, M. (1988). Electrophysiology of guinea-pig cerebellar nuclear cells in the *in vitro* brain stem-cerebellar preparation. *J. Physiol.* **404**, 241-258.
Lu, B., Yang, W., Dai, Q. and Fu, J. (2013). Using genes as characters and a parsimony analysis to explore the phylogenetic position of turtles. *PLoS ONE* **8**, e79348.
MacLean, R. A., Harms, C. A. and Braun-McNeill, J. (2008). Propofol anesthesia in loggerhead (*Caretta caretta*) sea turtles. *J. Wildlife Dis.* **44**, 143-150.
MacLeod, K. M. and Carr, C. E. (2005). Synaptic physiology in the cochlear nucleus angularis of the chick. *J. Neurophysiol.* **93**, 2520-2529.
Mancilla, J. G., Fowler, M. and Ulinski, P. S. (1998). Responses of regular spiking and fast spiking cells in turtle visual cortex to light flashes. *Vis. Neurosci.* **15**, 979-993.
Manley, G. A. (1970). Comparative studies of auditory physiology in reptiles. *J. Comp. Physiol. A* **67**, 363-381.
Manley, G. A. (2002). Evolution of structure and function of the hearing organ of lizards. *J. Neurobiol.* **53**, 202-211.
Manley, G. A. (2010). An evolutionary perspective on middle ears. *Hear. Res.* **263**, 3-8.
Marbey, D. and Browner, R. H. (1985). The reconnection of auditory posterior root fibers in the red-eared turtle, *Chrysemys scripta elegans*. *Hear. Res.* **1**, 1-4.
McAlpine, D., Jiang, D. and Palmer, A. R. (2001). A neural code for low-frequency sound localization in mammals. *Nat. Neurosci.* **4**, 396-401.
Miller, M. R. (1978). Scanning electron microscope studies of the papilla basilaris of some turtles and snakes. *Am. J. Anat.* **151**, 409-435.
Miller, M. R. and Kasahara, M. (1979). The cochlear nuclei of some turtles. *J. Comp. Neur.* **185**, 221-235.
Mori, K., Nowycky, M. C. and Shepherd, G. M. (1981). Electrophysiological analysis of mitral cells in the isolated turtle olfactory bulb. *J. Physiol.* **314**, 281-294.
Rice, M. E. and Nicholson, C. (1990). Glutamate- and aspartate-induced extracellular potassium and calcium shifts and their relation to those of kainate, quisqualate and N-methyl-D-aspartate in the isolated turtle cerebellum. *Neuroscience* **38**, 295-310.
Rodgers-Garlick, C. I., Hogg, D. W. and Buck, L. T. (2013). Oxygen-sensitive reduction in Ca^{2+}-activated K^+ channel open probability in turtle cerebrocortex. *Neuroscience* **237**, 243-254.
Rutishauser, U., Kotowicz, A. and Laurent, G. (2013). A method for closed-loop presentation of sensory stimuli conditional on the internal brain-state of awake animals. *J. Neurosci. Methods* **215**, 139-155.
Schnee, M. E., Lawton, D. M., Furness, D. N., Benke, T. A. and Ricci, A. J. (2005). Auditory hair cell-afferent fiber synapses are specialized to operate at their best frequencies. *Neuron* **47**, 243-254.
Schnee, M. E., Santos-Sacchi, J., Castellano-Muñoz, M., Kong, J.-H. and Ricci, A. J. (2011). Calcium-dependent synaptic vesicle trafficking underlies indefatigable release at the hair cell afferent fiber synapse. *Neuron* **70**, 326-338.
Schnee, M. E., Castellano-Munoz, M. and Ricci, A. J. (2013). Response properties from turtle auditory hair cell afferent fibers suggest spike generation is driven by synchronized release both between and within synapses. *J. Neurophysiol.* **110**, 204-220.
Shen, X.-X., Liang, D., Wen, J.-Z. and Zhang, P. (2011). Multiple genome alignments facilitate development of NPCL markers: a case study of tetrapod phylogeny focusing on the position of turtles. *Mol. Biol. Evol.* **28**, 3237-3252.
Sneary, M. G. (1988). Auditory receptor of the red-eared turtle: II. Afferent and efferent synapses and innervation patterns. *J. Comp. Neurol.* **276**, 588-606.
Soares, D. and Carr, C. E. (2001). The cytoarchitecture of the nucleus angularis of the barn owl (*Tyto alba*). *J. Comp. Neurol.* **429**, 192-205.
Szpir, M. R., Wright, D. D. and Ryugo, D. K. (1995). Neuronal organization of the cochlear nuclei in alligator lizards: a light and electron microscopic investigation. *J. Comp. Neurol.* **357**, 217-241.
Valverde, F. (1970). The Golgi method. A tool for comparative structural analyses. In *Contemporary Research Methods in Neuroanatomy* (ed. W. J. H. Nauta and S. O. E. Ebbesson), pp. 12-31. Berlin, Heidelberg: Springer.
van Hemmen, J. L., Christensen-Dalsgaard, J., Carr, C. E. and Narins, P. M. (2016). Animals and ICE: meaning, origin, and diversity. *Biol. Cybern.* **110**, 237-246.
Viete, S., Pena, J. L. and Konishi, M. (1997). Effects of interaural intensity difference on the processing of interaural time difference in the owl's nucleus laminaris. *J. Neurosci.* **17**, 1815-1824.
Wever, E. G. and Vernon, J. A. (1956a). The sensitivity of the turtle's ear as shown by its electrical potentials. *Proc. Natl. Acad. Sci. USA* **42**, 213-220.
Wever, E. G. and Vernon, J. A. (1956b). Sound transmission in the turtle's ear. *Proc. Natl. Acad. Sci. USA* **42**, 292-299.
Wever, E. G. and Vernon, J. A. (1956c). Auditory responses in the common box turtle. *Proc. Natl. Acad. Sci. USA* **42**, 962-965.
Willis, K. L., Christensen-Dalsgaard, J. and Carr, C. E. (2013a). Auditory brain stem processing in reptiles and amphibians: roles of coupled ears. In *Insights from Comparative Hearing Research* (ed. C. Köppl, G. A. Manley, A. N. Popper and R. R. Fay), pp. 193-225. New York: Springer.
Willis, K. L., Christensen-Dalsgaard, J., Ketten, D. R. and Carr, C. E. (2013b). Middle ear cavity morphology is consistent with an aquatic origin for testudines. *PLoS ONE* **8**, e54086.
Willis, K. L., Johny, A. and Carr, C. E. (2014). *Tonotopic organization of the turtle brain stem. Program No. 431.09 2014 Neuroscience Meeting Planner*. Washington, DC: Society for Neuroscience, 2014. Online. http://bit.ly/2vnhBHn.
Wu, Y.-C. and Fettiplace, R. (1996). A developmental model for generating frequency maps in the reptilian and avian cochleas. *Biophys. J.* **70**, 2557-2570.
Yin, T. C. and Kuwada, S. (1983). Binaural interaction in low-frequency neurons in inferior colliculus of the cat. III. Effects of changing frequency. *J. Neurophysiol.* **50**, 1020-1042.

Table S1. Results of varying the experimental temperature and ACSF recipe.

Number of Units	Temperature (°C)	ACSF Recipe
6	18	Avian
7	18	Avian
2	18	Rodgers-Garlick, et al
2	18	Fettiplace & Crawford
8	18	Fettiplace & Crawford
6	18	Fettiplace & Crawford
0	18	Fettiplace & Crawford
1	18	Rice & Nicholson
4	18	Rice & Nicholson
0	18	Rice & Nicholson
16	20	Connors & Kriegstein
12	20	Connors & Kriegstein
7	22	Connors & Kriegstein
8	22	Connors & Kriegstein
16	22	Connors & Kriegstein
12	23	Connors & Kriegstein
30	24	Connors & Kriegstein